

An Ultrafast Lithium-ion Battery with Long-term Cycling Performance Based on Hard Carbon

Manqin Tang¹, Dan Zhao², Jing Li^{1,*}, Pengyu Li¹, Jidong Duan¹, Rui Wang¹, Jinhan Teng¹, Chun Yuan³

¹ State Key Laboratory of Environmentally Friendly Energy Materials, School of Materials, Science and Engineering, Southwest University of Science and Technology, Mianyang 621010, China.

² Sichuan Lvxin Power Technology Co. Ltd, Suining 629000, China.

³ Gansu Jinchuan Group co. Ltd, Jinchang, 737100, China

*E-mail: xy13787103391@126.com

Received: 4 January 2021 / Accepted: 17 February 2021 / Published: 28 February 2021

In this work, we construct lithium-ion batteries (LIBs) with capacitive-level cycling performance and ultrafast charge/discharge via electrode engineering. Two typical battery-type materials are used, namely, $\text{LiNi}_{0.6}\text{Co}_{0.2}\text{Mn}_{0.2}$ as the cathode material and hard carbon (HC) without pre-lithiation as the anode material. In addition to the reasonable electrode design, it is concluded after analysing the energy storage mechanism that the capacitive-controlled storage behaviour of HC materials in a full cell configuration is the major reason that the device exhibits superior cycling performance. By conducting a galvanostatic charge/discharge cycling test of a 144 mAh battery at 10C ($t_{\text{charge}}/t_{\text{discharge}} \approx 4.8$ min), the capacity retention rate of the battery is 99.36% after 32000 cycles. The specific energy reaches $43.59 \text{ Wh}\cdot\text{kg}^{-1}$ at $42.01 \text{ W}\cdot\text{kg}^{-1}$ within a discharge time of 67.3 s, while the energy density is $29.55 \text{ Wh}\cdot\text{kg}^{-1}$ at $1580.81 \text{ W}\cdot\text{kg}^{-1}$; these values are calculated based on the weight of the whole device. This work expands the application range of HC materials in the field of batteries.

Keywords: lithium-ion battery, hard carbon, cycle life, $\text{LiNi}_{0.6}\text{Co}_{0.2}\text{Mn}_{0.2}$, ultra-fast charge/discharge

1. INTRODUCTION

With the depletion of energy, the research of electrochemical energy storage devices with high energy and power density and long cycling life has attracted the interests of many researchers. Supercapacitors (SCs), based on active capacitive materials, have ultra-long cycling lives (>10000) and high power densities but low energy densities, while lithium-ion batteries (LIBs) based on battery-type active materials have high energy densities but low power densities and poor cycling performances (500~1000) [1-8]. However, in recent years, a newly developed energy storage device, hybrid lithium-ion energy devices (LICs), have the advantages of both LIBs and SCs, demonstrating long cycling lives

(>10000) and high energy densities (20~100 Wh·kg⁻¹); these LICs are constructed with battery-type and capacitive materials [9-11].

Generally, the negative electrode of LICs is pre-lithiated hard carbon (HC), which is mainly composed of disordered carbon layers, with many defects and pores. Certainly, its lithium storage is isotropic and can withstand the impact of high current, so it can be used in places that require high current charge and discharge [12]. High-power lithium-ion batteries that use HC materials as anode electrodes have also been applied in electric vehicles. However, HC materials have not only a low first Coulombic efficiency and a dismal cycling life but also an unclear lithium storage mechanism, which hinders their use in LIBs with ultra-fast charge and discharge.

To improve electrochemical performance, in addition to the research of electrode materials, it is also necessary to optimize the design of the device manufacturing process. In terms of electrode materials, the reports are mainly aimed at designing novel structures or developing new materials [13-15]. Clearly, research on the optimization of fabrication is more helpful for industrialized devices. The reasonable design of the negative/positive capacity ratio (N/P ratio) in an energy storage device can improve the cycling and rate performances [16-19]. Moreover, the adjustment of electrode thickness, number of voids and formulation, as well as the use of different electrode mixing sequences, can all enhance the performance of an electrochemical energy storage system [20-27].

Herein, we use commercialized LiNi_{0.6}Co_{0.2}Mn_{0.2} (NCM622) as the cathode material and commercialized HC without pre-lithiation as the anode material to build a battery. The assembled device acts as an lithium-ion battery (LIB) with capacitive-level cycling performance and ultra-fast charge/discharge. We first verify the electrochemical characteristics of the battery in a coin cell setup and further evaluate the electrochemical performance in a pouch cell configuration. By discussing the energy storage mechanism of the HC materials, it is proven that the energy storage kinetics of the lithium ions in the HC materials can be mainly defined as capacitance at high current densities, which is more suitable for high-power energy storage devices. In addition, the reasonable N/P ratio design and the low mass loading of the electrodes can also make the battery have long cycling stability at high current densities as well as at high power and energy densities [7,16-19]. This device blurs the boundary between LIBs and SCs, but introduces devices with high energy and power densities as a new research idea to study.

2. EXPERIMENTAL

NCM622 (T61R) was purchased from Hunan Shanshan Energy Technology Co., Ltd., China, with $D_{50}=13.058\ \mu\text{m}$ and $S_{\text{BET}}=0.34\ \text{m}^2\cdot\text{g}^{-1}$. HC (KURANODE Type 2) was provided by KURARAY CO., Ltd. Japan, with $D_{50}=5\ \mu\text{m}$ and $S_{\text{BET}}=7\ \text{m}^2\cdot\text{g}^{-1}$. All the materials were used directly after vacuum baking.

2.1 Morphological characterization

The crystal structures of the active materials were obtained by X-ray diffraction (XRD) using X'Pert pro, PANalytical with a Cu-K α radiation source at 50 kV and 200 mA and a range of 3° to 80°

(2θ) with a 0.03° step width. The surface morphologies of the materials were recorded by field-emission scanning electron microscopy (FE-SEM, Ultra55, Carl Zeiss NTS GmbH).

2.2 Electrode preparation

To prepare the cathode electrode NCM622, conductive carbon black (Super P Li, SP), Ketjen black (ECP600JD) and polyvinylidene fluoride (PVDF 5130) were whisked together at a weight ratio of 90:3:2:5. Then, n-methyl-pyrrolidone (NMP) was added as the solvent to the mixture, stirred into an electrode slurry, and cast onto 16 μm -thick aluminium foil. Finally, vacuum baking was performed at 120°C to remove the solvent. The double-sided mass loading of the cathode electrode was $10.80\text{ mg}\cdot\text{cm}^{-2}$. The materials for preparing the anode electrode were weighed according to the following mass ratio of HC:SP:CMC (sodium carboxymethylcellulose, CMC2200):SBR (styrene butadiene rubber)=92.8:2:1.2:4. First, CMC was dissolved in deionized water to form a transparent viscous liquid, and the remaining materials were then added to the mixture and blended well. Next, the mixture was coated on 8 μm -thick copper foil. The anode electrode was dried thoroughly at 110°C . The double-sided mass loading of the HC electrode was $8.65\text{ mg}\cdot\text{cm}^{-2}$. After drying, the anode and cathode electrodes were pressed to an appropriate thickness through a cold roller press. The cathode electrode density was $3.2\text{ g}\cdot\text{cm}^{-3}$, and the anode electrode density was $0.9\text{ g}\cdot\text{cm}^{-3}$. Then, the single-sided coated laminates were punched into 15 mm-diameter electrode discs for the coin battery (CR2032). The double-sided coated electrodes of the pouch cells were cut into rectangles by a paper knife in which the size of the cathode electrode was $300\text{ mm} \times 40\text{ mm}$ and the anode electrode was $350\text{ mm} \times 42\text{ mm}$, as shown in Fig. 1a. Then, the cut electrode slices were baked in a vacuum oven at 80°C for later use.

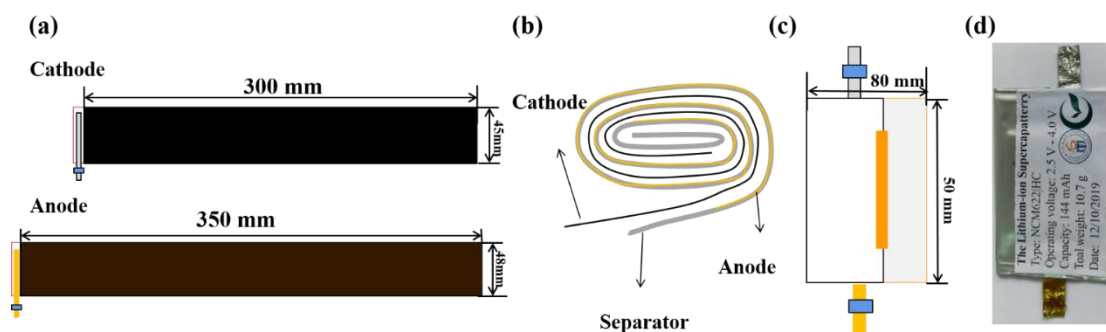


Figure 1. (a) Electrode slice size, (b) schematic diagram of the wound cell interior, (c) schematic diagram of the wound cell; and (d) photograph of the assembled pouch cell.

2.3 Cell assembly and electrochemical measurements

Half cells of the anode and cathode materials and coin-type full cells were assembled in a glove box with an argon atmosphere. Half cells were made of 16.5 mm lithium metal foil as the opposite electrodes, a Celgard 2500 separator, and an electrolyte in which 1 M LiPF_6 was dissolved in a mixture of ethylene carbonate (EC)/dimethyl carbonate (DMC)/ethyl methyl carbonate (EMC) at a volume ratio

of 1:1:1. NCM and HC electrodes with the same size were assembled for the coin-type full cells in the same way as the half-cells. The voltage window of the NCM half battery was (3.0-4.2 V), the anode electrode was (0.005-2.0 V), and the full cell was (2.5-4.0 V). CV (cyclic voltammetry) tests were conducted after 3 cycles at 0.1C.

The two-electrode pouch full cells were carried out in a drying room with a dew point below -45 °C. The cell was wound in the following structure, anode plate-separator-cathode plate-separator, and the schematic diagram is shown in Fig. 1b and c. The cell was then placed in an aluminium-plastic bag, further dried and dehydrated, and injected with the same kind of electrolyte as the coin cell. Fig. 1d shows a photograph of the assembled pouch cell. A lithium metal reference electrode was used on the outermost layer of the cell to monitor the cathode and anode potential changes in the pouch battery during the constant current charge/discharge cycles.

3. RESULTS AND DISCUSSION

3.1 Microstructure of the materials

The SEM images and the XRD curves of NCM622 and HC are plotted in Fig. 2, and it can be seen that the NCM622 powders we purchased are secondary spherical particles in a typical layered structure piled up by small particles, while HC is an amorphous material with an irregular shape. In terms of the microstructures, it is helpful for us to construct an energy storage device in the fast charging system.



Figure 2. SEM images of (a) NMC622 and (b) HC and (c) XRD patterns of NMC622 and HC.

3.2 Device construction and energy storage mechanism analysis

Fig. 3 shows the electrochemical performance of the different types of coin cells, including the NCM622|Li, HC|Li, and NCM622|HC test cells. The NCM622 material is a typical battery material with a reduction and oxidation peak ($\text{Ni}^{2+} \leftrightarrow \text{Ni}^{3+} \leftrightarrow \text{Ni}^{4+}$) [15] at 3.68 V and 3.86 V, respectively, in the CV (Fig. 3a) and charge/discharge curves (Fig. 3d). As shown in Fig. 3d, the first charge specific capacity is $190.85 \text{ mAh}\cdot\text{g}^{-1}$ at 0.1C, and the reversible specific capacity is $172.13 \text{ mAh}\cdot\text{g}^{-1}$, for which the first coulombic efficiency is up to 90.19%. Different from the typical shape of battery-type materials, the CV

curve of HC in Fig. 3b has a relatively wide peak, and the charge/discharge curves in Fig. 3e are composed of sloping regions and a plateau. Although there are still much controversy about the Li^+ storage mechanism in HC materials, the adsorption mechanism in the slope areas and the insertion mechanism in the slope areas are widely accepted [28,29]. The reversible specific capacity at 0.1C can reach $229.17 \text{ mAh}\cdot\text{g}^{-1}$, while the first coulombic efficiency is only 79.89% because of the micropores on the surface of the HC materials. According to the specific capacity of the anode and cathode materials for the first cycle, we designed the N/P ratio of the full battery using Eq. S1. The specific capacity of the NCM622 electrode is calculated to be $190 \text{ mAh}\cdot\text{g}^{-1}$, which is its first charge specific capacity, and the specific capacity of the HC electrode is calculated to be $250 \text{ mAh}\cdot\text{g}^{-1}$, that is, the discharge from the open-circuit potential to 0.05 V. In this paper, the N/P value is 1.1 to ensure that this device can withstand a large current.

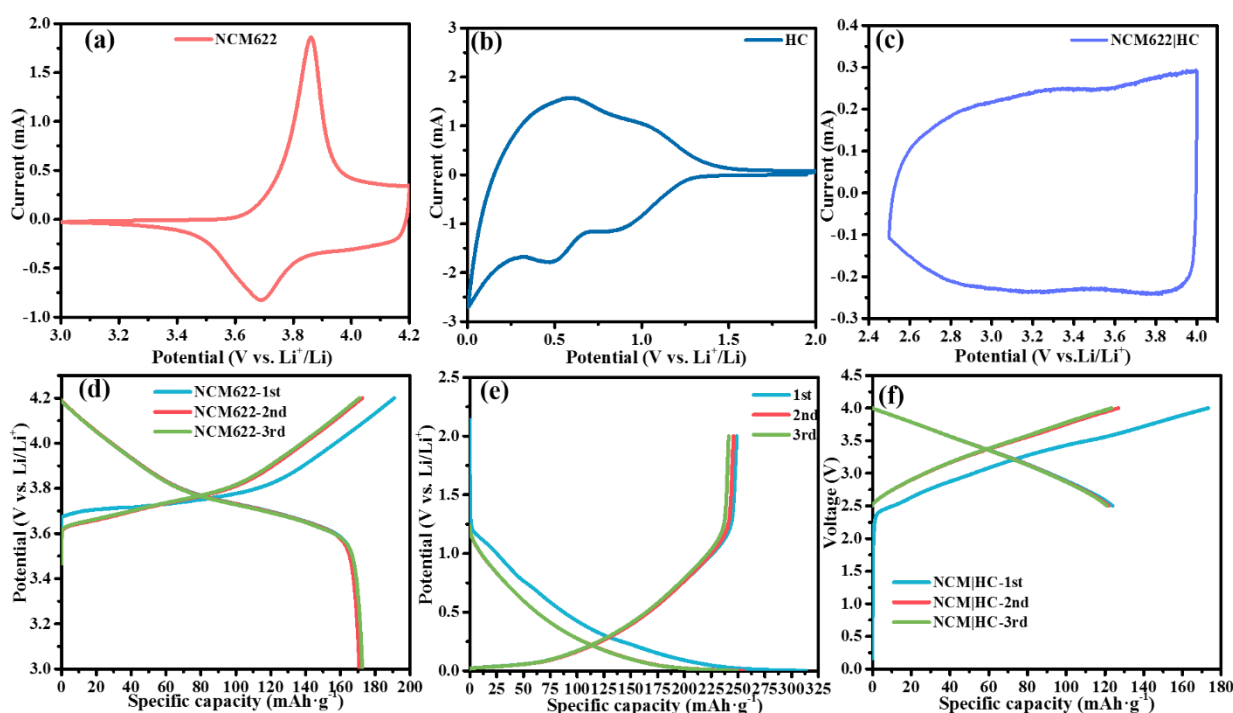


Figure 3. Electrochemical characteristics of coin cells: the CV curves of (a) NCM622, (b) HC and (c) NCM|HC recorded at $0.1 \text{ mV}\cdot\text{s}^{-1}$ and the charge/discharge curves of (d) NCM622, (e) HC and (f) NCM|HC recorded at 0.1C.

As shown in Fig. 3c, the CV curve of the coin-type full battery displays a rectangular shape without distinct cathodic/anodic peaks, which is similar to the result of the energy storage system constructed by Jon Ajuria et al. [30]. Moreover, as shown in Fig. 3f, the well-defined linear shape of the charge/discharge profiles also indicates a similar situation in the supercapacitor. The reversible specific capacity of the device is $123.95 \text{ mAh}\cdot\text{g}^{-1}$ at 0.1C based on the mass of the cathode material, and the first coulombic efficiency is only 71.54%. Moreover, the influence of the different voltage windows on the electrochemical performance is illustrated in Fig. S1. In the voltage range of 2.8-4.0 V, its capacitance characteristic is more obvious, but it has a lower specific capacity. Whereas during the voltage range of

2.5-4.2 V, a higher cut-off voltage affects the rate performance and cycling stability. Therefore, we chose the voltage range of 2.5-4.0 V for the follow-up study.

3.3 Electrochemical performance of the pouch cell

To further verify the practicality of this energy storage system, we made a roll-up pouch cell with a capacity of 144 mAh. Fig. 4a shows the CV curve of the pouch full cells. Similar to the coin-type full cell, the CV curve has no obvious peak during the voltage range of 2.5-4.0 V, which is similar to the curve of a supercapacitor. Fig. 4b shows that the cell has a triangular charge/discharge curve at a current of 144 mA. This result is an interesting phenomenon that shows capacitance in the battery device.

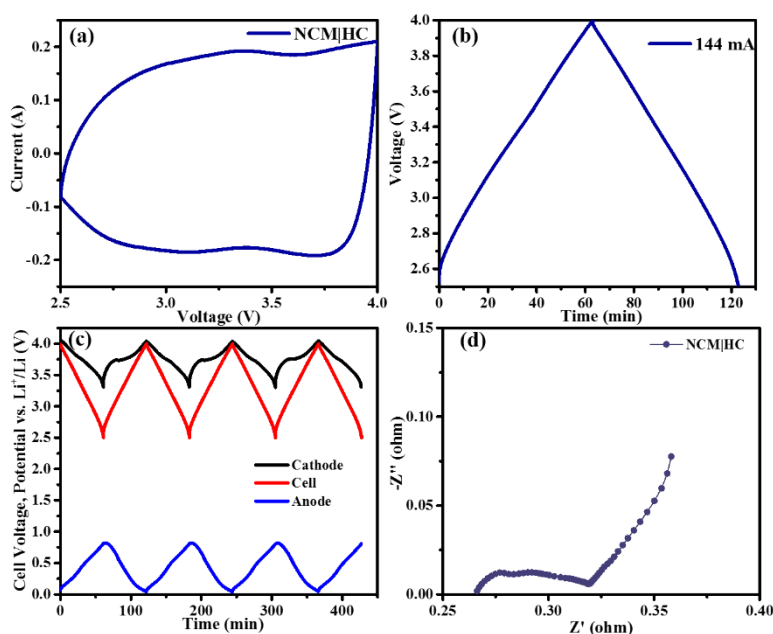


Figure 4. Electrochemical characteristics of pouch cells: (a) CV curve of the pouch cell at $0.5 \text{ mV} \cdot \text{s}^{-1}$, (b) galvanostatic charge/discharge curves of the pouch cell at 144 mA, (c) galvanostatic charge/discharge profiles for three-electrode full cells in the voltage range of 2.5-4.0 V, and (d) EIS curves of the cell.

Three-electrode experimental pouch cells were used to analyse the potential change of the anode and cathode electrodes with respect to lithium metal during charge and discharge at a current density of 1C. As shown in Fig. 4c, when the cell is cycled in the range of 2.5-4.0 V, the potential range of the cathode electrode is between 3.30 V to 4.04 V, while the anode electrode is between 0.04 V to 0.80 V. The highest potential of the positive electrode material is exactly 4.04 V vs. Li^+/Li , and the cathode material decays rapidly, exceeding this potential. Simultaneously, the lowest potential ($>0 \text{ V}$ vs. Li^+/Li) of the anode electrode prevents the deposition of metallic lithium in the system, and the potential range of the HC electrode is exactly in the region where HC has fast reaction dynamics, which ensures that the system has fast charge/discharge characteristics [31]. Electrochemical impedance spectroscopy (EIS) is

shown in Fig. 4d. The low value that is observed should be the cause of the previously described electrochemical properties.

The rate performance of the pouch cells is plotted in Fig. 5a and b. The capacity of the system at a current of 1C (144 mA) is 144 mAh, and the specific capacity of the material can reach $117.21 \text{ mAh}\cdot\text{g}^{-1}$. When charged and discharged at 40C (5760 mA), the capacity is still 68.6 mAh. The capacity retention rate is up to 47.64%, and the CE still reaches 99%. However, due to the influence of polarization at a high current, the charge/discharge curve in Fig. 5b is no longer a straight line at 40C. Notably, after the different rate tests, the device can recover 98% of the capacity at a current of 144 mA. In addition to the choice of anode and cathode materials, the good rate performance of the energy storage device is more so due to the fast Li^+ transmission at a low mass loading of the electrode.

The high-rate cycling stability of the two-electrode experimental pouch cells is illustrated in Fig. 5c at a current of 1440 mA (10C, $t_{\text{charge}}/t_{\text{discharge}} \approx 4.8 \text{ min}$). After 32000 cycles, the capacity retention rate is 86.64%, and the coulombic efficiency is also above 99%. Fig. 6d shows the chronopotentiometry curves at different cycles. After 32000 cycles, a good linear relationship is maintained between the test time and cell voltage. The ultra-long cycling performance during fast charge and discharge is surprising and exceeds our understanding of classical lithium-ion battery systems based on battery-type active materials. Hence, this result seems to be explained by the capacitive-like behaviour of an energy storage mechanism. The deeper principles need to be explored with further research.

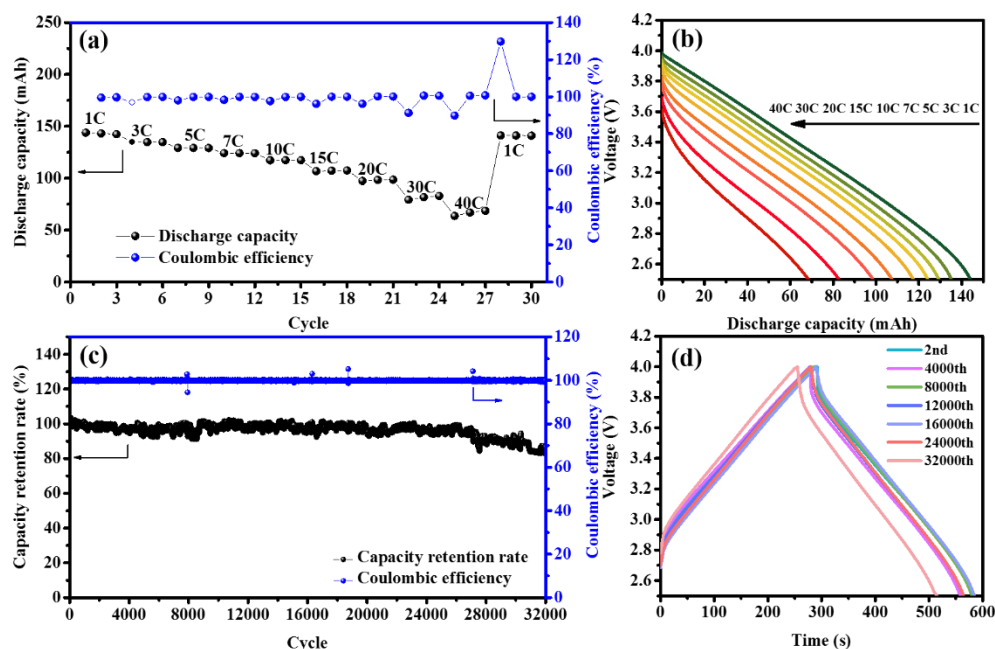


Figure 5. Electrochemical performance of the pouch cell: (a) rate performance, (b) galvanostatic discharge curves at different current densities, (c) cycling performance at 10C, and (d) galvanostatic charge/discharge curves for different cycles at 10C.

The Ragone plot in Fig. 6 shows the relationship between the power density and energy density of the NCM|HC system. When the power density is $42.02 \text{ W}\cdot\text{kg}^{-1}$, the mass energy density is 43.59

Wh·kg⁻¹, which is calculated based on the weight of the whole device (using Eqs. S6 and S7), while the specific energies of the SCs are 5-10 Wh·kg⁻¹ within a discharge time of 67.3 s, the mass energy density can reach 29.55 Wh·kg⁻¹ at 1580 W·kg⁻¹. However, the small capacity of the pouch cell reduces the power and energy density. Table 1 shows the electrochemical performances of our system compared with other reported energy storage systems.

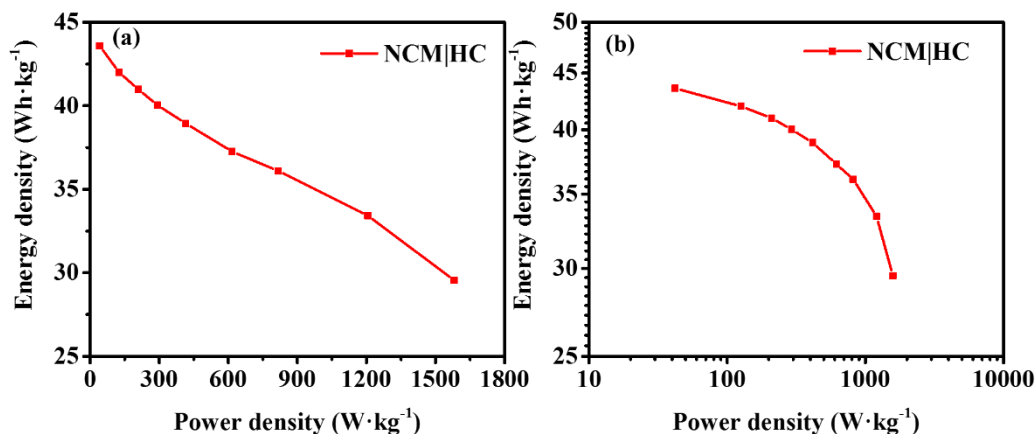


Figure 6. Ragone plot details of the pouch cell

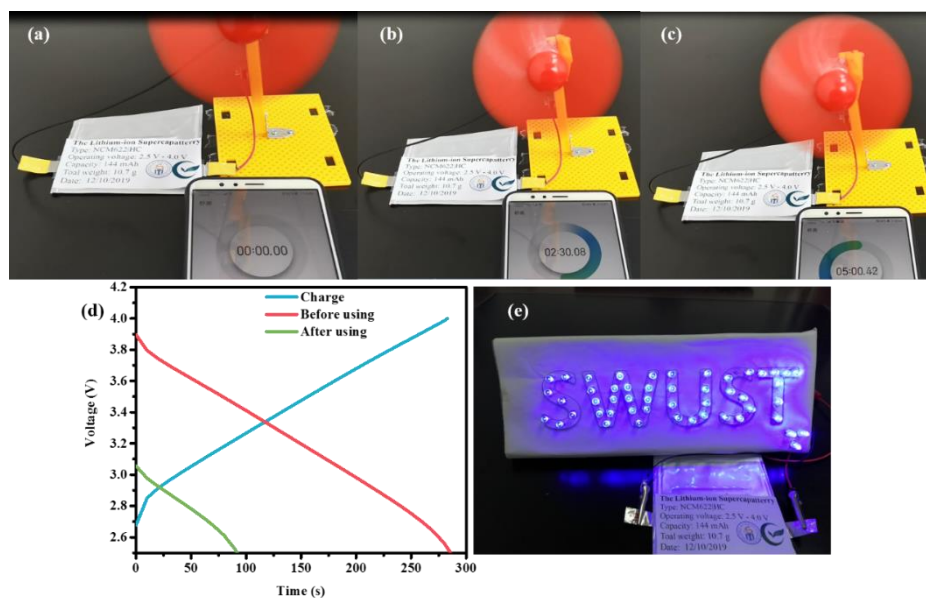


Figure 7. Practical application of the pouch: (a-c) fans driven by the pouch cell after charging at 10C for 5 min, (d) galvanostatic charge/discharge curves during the actual application at 10C, and (e) graphic composed of lit LED lights

We also applied the battery for practical use. Fig. 7a-c shows the picture of the device driving a small fan for 5 min (the motor power is approximately 4 W) while the cell is charged in a voltage range

of 2.5 V -4.0 V at a current of 10C. Fig. 7d shows the charge/discharge curve at a 10C current before and after the battery is used. After 5 min, the capacity of the cells is still 20 mAh, showing a capacity retention rate of 39%. Fig. 8e is a picture of five letters, "SWUST", and a "heart" shape composed of 50 lit LED lights that are connected in series with the device. Therefore, it can be determined that the device still has very good application prospects under fast charging conditions.

Table 1. Electrochemical performances of our system compared with other reported energy storage systems

Electrodes	Type	Voltage (V)	Specific energy (Wh•kg ⁻¹)	Cyclability	Ref.
NCM523/AG	LIB	3.0-4.3	/	1C/4700/92%	32
NCM523/AG	LIB	3.0-4.15	/	6C/600/86%	33
NMC523/HC	LIB	/	/	6C/800/91%	34
LFP+AC/Li doped HC	LIC	2.2-3.8	30	60C/30000/90%	35
NCM523+AC/Graphite	LIC	2.5-4.0	36.2	1C/1000/95%	36
NCM622/HC	LIB	2.5-4.0	43.59	10C/32000/86.64%	This work

3.3 Energy storage mechanism analysis of the anode electrode

To explore the reason for the electrochemical behaviour produced by this energy storage device, the energy storage mechanism of the anode electrode is discussed in Fig. 8. Since the boundary between the capacitive and battery-type materials is not obvious enough, Dunn et al. [37] calculated the contributions of the two charge storage mechanisms using CV curves to distinguish them. Herein, we use this method to analyse the energy storage mechanism of the HC materials, which is still controversial due to its complex structure. The linear relationship of the response currents at the P1, P1', P2 and P2' potentials and at different scanning rates is fitted by Fig. 8a, and the results are shown in Fig. 8b. All fitting results are $b > 0.5$ (using Eqs. S2-S5), indicating that the Li⁺ storage kinetics of the HC materials are controlled by capacitive behaviour, which means a fast Li⁺ transport mechanism. In addition, at approximately 0.9 V vs. Li⁺/Li, the b value of 1 represents fast near-surface activity. Moreover, the proportion of capacitive-controlled and diffusion-controlled processes at each scanning speed is calculated. Fig. 8c reveals the proportion of capacitive control in regard to the overall capacity at 0.7 mV•s⁻¹. As shown in Fig. 8d, with an increasing sweep rate from 0.1 mV•s⁻¹ to 1 mV•s⁻¹, the proportion of the capacitive control process increases from 77.53% to 96.39%. Therefore, combined with the whole process of battery design, we think that the capacitive behaviour of the energy storage system is caused by the HC materials at a low mass loading. The HC materials have fast reaction kinetics during charge and discharge, and the thin electrodes allow Li⁺ to be transported quickly. Similar discussion results

were mentioned by Yang et al. [27] and Li et al. [28]. They thought adsorption was the main form of lithium storage throughout the investigated potential range.

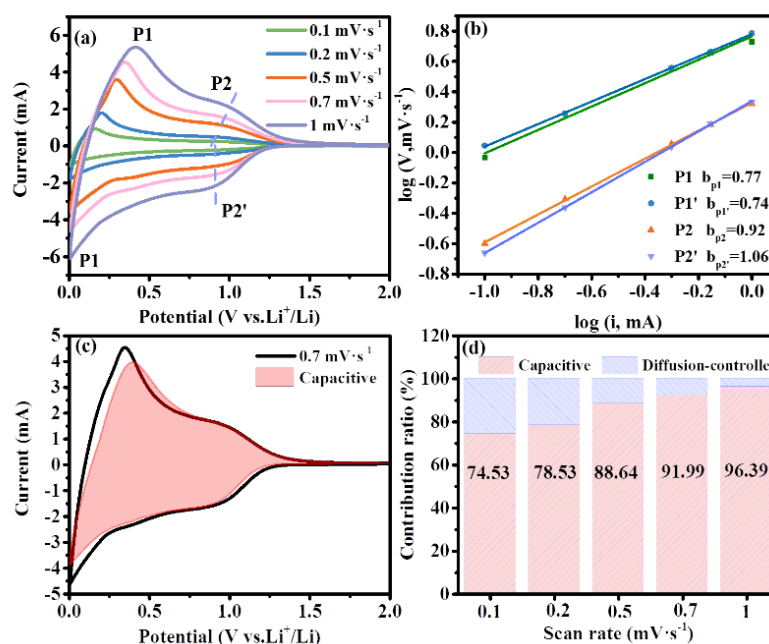


Figure 8. (a) CV curves of the HC material at various scan rates from 0.1 to 1 mV·s⁻¹ and (b) the dependence of the response current on the scan rate, (c) contribution of the capacitive and diffusion process at the scan rate of 0.7 mV·s⁻¹, and (d) contribution ratios of the capacitive-controlled process at different scan rates.

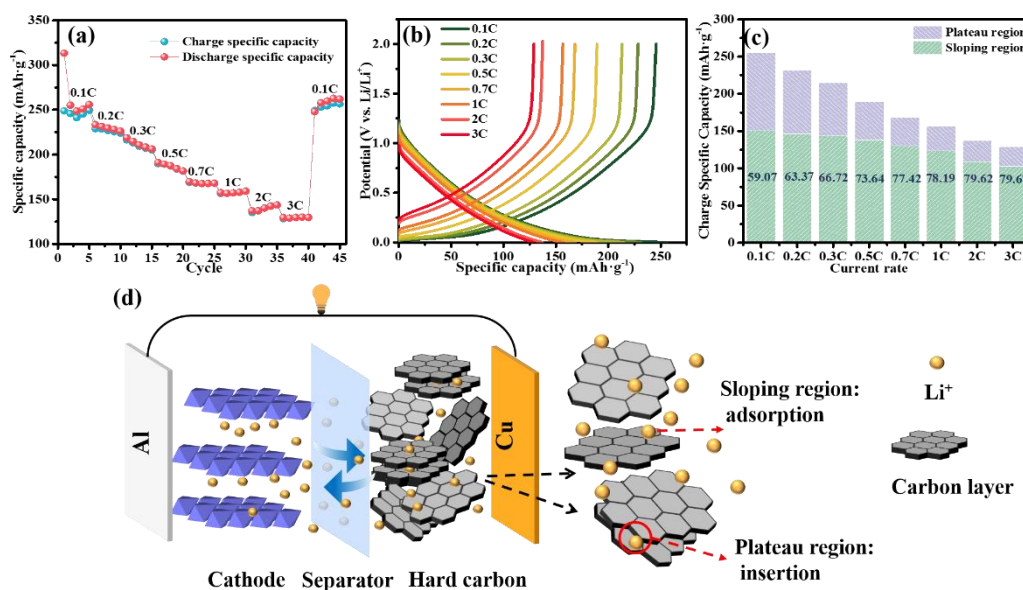


Figure 9. (a) Rate performance, (b) galvanostatic charge/discharge curves and (c) discharge specific capacities at different potential ranges obtained from (b) the HC material at various current densities from 0.1C to 3C. (d) Mechanism of the HC cell.

To gain further insights into the Li^+ transfer behaviour of HC, we discuss in detail the rate performance of the anode half-cell in Fig. 9 From Fig. 9a-c, we find that the excellent rate performance of HCs is mainly contributed by the capacity of the slope area (0.05-2.0 V). The capacity contribution of the slope area is increased from 59.07% to 79.67% when the current density is increased from 0.1C to 3C. This result further indicates that HC undergoes a capacitive-controlled process at high currents, and a large number of studies show that adsorption lithium storage mainly occurs in the slope area, while insertion lithium storage occurs in the plateau area (0.001-0.05 V), as depicted in Fig. 9d. As our three electrode test results show, our reasonable design of the N/P ratio provides the anode voltage range to be just inside the slope range, which explains why the device has excellent cycling and rate performances.

4. CONCLUSION

In this work, an energy storage system is constructed with two typical battery-type materials based on the Faraday reaction, NCM622 as the cathode material and HC as the anode material. The resulting system exhibits a long life during fast charge and discharge cycling and an excellent rate capability. Under the condition of sacrificing a certain mass power density, the decreased mass loading of the electrodes to produce thin electrodes and the choice of a reasonable N/P value enabled the energy storage device to demonstrate a capacity retention of 86.64% after 32000 cycles at 10C, a well-defined linear shape of the charge/discharge profiles, and rectangular-shaped CV curves, which are the characteristics of a supercapacitor. We assume that the thickness of the electrode ensured fast Li^+ transport, and the reasonable N/P value ensured that there would be no growth of lithium dendrites during the test process. The main reason, of course, was that the energy storage mechanism of the anode material was surface-controlled behaviour. In conclusion, this work expands the application range of HC materials in the field of batteries, and the cycling life blurs the boundary between supercapacitors and batteries.

SUPPORTING MATERIALS

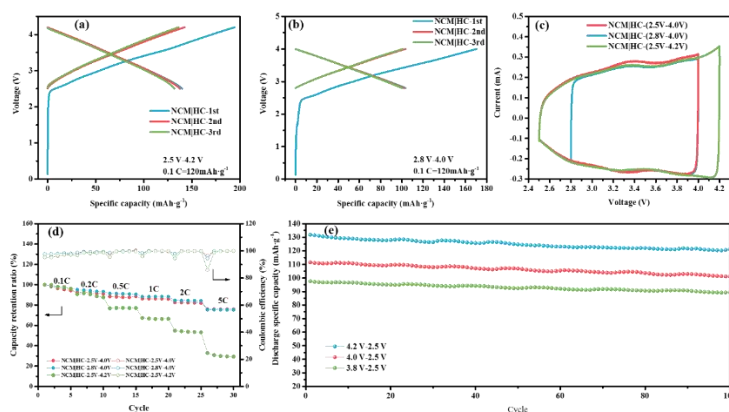


Figure S1. Electrochemical performance of the supercapattery in different voltage windows: charge/discharge curves from 2.5 V-4.2 V (a) and 2.8 V-4.0 V (b), CV curves (c), rate performance (d), and cycling performance (e).

Equation:

Eq. S1: The N/P ratio is calculated with the following equation:

$$\frac{N}{P} = \frac{C_{\text{discharge-anode}} \times m_{\text{anode loading}}}{C_{\text{charge-cathode}} \times m_{\text{cathode loading}}} \quad (\text{S1})$$

Eqs. S2 and S3: The voltammetric response obeys a power-law relationship of the measured current (i, mA) with the sweep rate (v, mV s⁻¹):

$$i = a v^b \quad (\text{S2})$$

$$\log i = \log a + b \log v \quad (\text{S3})$$

Eqs. S4 and S5: The capacitive contribution can be quantified by separating the current response i at a fixed potential V into capacitive reactions (k₁ v) and diffusion-controlled processes (k₂ v^{1/2}) with the following equations:

$$i(V) = k_1 v + k_2 v^{1/2} \quad (\text{S4})$$

$$i(V)/v^{1/2} = k_1 v^{1/2} + k_2 \quad (\text{S5})$$

Eq. S6: The energy density (E) is calculated with the following equation:

$$E = I \int U dt / m \quad (\text{S6})$$

where I is the current, U represents the cell voltage, and m is the mass of the whole cell.

Eq. S7: The power density (P) is calculated with the following equation:

$$P = E/t \quad (\text{S7})$$

ACKNOWLEDGMENT

This work was supported by the National Key Research and Development Programme of China (2018YFB0104204).

References

1. R. Kötzt, M. Carlen, *Electrochim. Acta*, 45 (2000) 2483-2498.
2. W. Raza, F. Ali, N. Raza, Y. Luo, K. Kim, J. Yang, S. Kumar, A. Mehmmod, E. Kwon, *Nano Energy*, 52 (2018) 441-473.

3. S. Yang, Y. Liu, Y. Hao, X. Yang, W. Goddard III, X. Zhang, B. Cao, *Adv. Sci.*, 5 (2018) 1700659.
4. H. Lu, L. He, X. Li, W. Zhang, J. Che, X. Liu, Z. Hou, H. Du, Y. Qu, *J. Mater. Sci.: Mater. Electron.*, 30 (2019) 13933–13938.
5. F. Wu, J. Maier, Y. Yu, *Chem. Soc. Rev.*, 49 (2020) 1569-1614 .
6. A.M. Colclasure, A.R. Dunlop, S.E. Trask, B.J. Polzin, A.N. Jansen, K. Smith, *J. Electrochem. Soc.*, 166 (2019) A1412-A1424.
7. H. Kang, C. Lim, T. Li, Y. Fu, B. Yan, N. Houston, V.D. Andrade, F.D. Carlo, L. Zhu., *Electrochim. Acta*, 232 (2017) 431-438.
8. A. Yiitalp, A. Tademir, S.A. Gürsel, A. Yürüm, *Energy Storage*, 2 (2020) e154.
9. X. Yu, J. Deng, C. Zhan, R. Lv, Z.H. Huang, F. Kang, *Electrochim. Acta*, 228 (2017) 76-81.
10. D.M. Chen, S.Q. Sun, G.X. Yu, L.G. Qin, W.J. Wang, M.Y. Jiang, J. Chen, *Carbon*, 166 (2020) 91-100.
11. R. Lu, X. Ren, C. Zhan, C. Wang, R. Lv, W. Shen, F. Kang, Z. Huang, *J. Alloy. Compd.*, 835 (2020) 155398.
12. J. Ni, Y. Huang, L. Gao, *J. Power Sources*, 223 (2013) 306-311.
13. L. Yang, K. Yang, J. Zheng, K. Xu, K. Amine, F. Pan, *Chem. Soc. Rev.*, 49 (2020) 4667-4680.
14. H. Kim, M. Kim, H. Jeong, H. Nam, J. Cho, *Nano Lett.*, 15 (2015) 2111-2119.
15. J. Fu, D. Mu, B. Wu, J. Bi, H. Cui, H. Yang, H. Wu, F. Wu, *ACS Appl. Mater. Interfaces*, 10 (2018) 19704-19711.
16. Y. Abe, S. Kumagai, *J. Energy Storage*, 19 (2018) 96-102.
17. F. Reuter, A. Baasner, J. Pampel, M. Piwko, S. Dörfler, H. Althues, S. Kaskel, *J. Electrochem. Soc.*, 166.14 (2019) A3265-A3271.
18. C. Kim, K. Jeong, K. Kim, C. Yi, *Electrochim. Acta*, 155 (2015) 431-436.
19. B. Son, M. Ryou, J. Choi, S. Kim, J. Ko, Y. Lee, *J. Power Sources*, 243 (2013) 641-647.
20. C. Heubner, A. Nickol, J. Seeba, S. Reuber, N. Junker, M. Schneider, A. Michaelis, *J. Power Sources*, 419 (2019) 119-126.
21. R. Ciez, D. Steingart, *Joule*, 4 (2020) 597-614..
22. H. Dreger, W. Haselrieder, A. Kwade, *J. Energy Storage*, 21 (2019) 231-240.
23. D. Miranda, A. Gören, C. Costa, M. Silva, A. Almeida, S. Lanceros-Méndez, *Energy*, 172 (2019) 68-78.
24. K. Park, S. Myeong, D. Shin, C.-W. Cho, S.C. Kim, T. Song, *J. Ind. Eng. Chem.*, 71 (2019) 270-276.
25. G.W. Lee, J.H. Ryu, W. Han, K.H. Ahn, S.M. Oh, *J. Power Sources*, 195 (2010) 6049-6054.
26. Y., Cao, M. Li, J. Lu, J. Liu, K. Amine, *Nat. Nanotechnol.*, 14 (2019) 200-207.
27. D. Bhattacharjya, D. Carriazo, J. Ajuria, A. Villaverde, *J. Power Sources*, 439 (2019) 227106.
28. G. Yang, X. Li, Z. Guan, Y. Tong, B. Xu, X. Wang, Z. Wang, L. Chen, *Nano Lett.*, 20 (2020) 3836-3843.
29. R. Li, J. Huang, J. Li, L. Cao, X. Zhong, A. Yu, and G. Lu, *J. Electroanal. Chem.*, 862, (2020) 114044.
30. J. Ajuria, F. Aguesse, *Electrochim. Acta*, 334 (2020) 135587.
31. L. Jin, X. Guo, C. Shen, N. Qin, J. Zheng, Q. Wu, C. Zhang, J.P. Zheng, *J. Power Sources*, 441 (2019) 227211.
32. Y. Liu, J. Harlow, J. Dahn, *J. Electrochem. Soc.*, 167 (2020) 020512.
33. K. Chen, M. Namkoong, V. Goel, C. Yang, S. Kazemiabnavi, S. Mortuza, E. Kazyak, J. Mazumder, K. Thornton, J. Sakamoto, N. Dasgupta, *J. Power Sources*, 471 (2020) 228475.
34. L. Hu, G. Cheng, F. Wang, J. Ren, *Int. J. Electrochem. Sci.*, 14 (2019) 2804-2814.
35. L. Jin, J. Zheng, Q. Wu, A. Shellikeri, S. Yturriaga, R. Gong, J. Huang, J.P. Zheng, *Materials Today Energy*, 7 (2018) 51-57.
36. X. Sun, X. Zhang, B. Huang, H. Zhang, D. Zhang, and Y. Ma. *J. Power Sources*, 243 (2013) 361-368.

37. P. Simon, Y. Gogotsi, B. Dunn, *Science*, 343 (2014) 1210-1211.

© 2021 The Authors. Published by ESG (www.electrochemsci.org). This article is an open access article distributed under the terms and conditions of the Creative Commons Attribution license (<http://creativecommons.org/licenses/by/4.0/>).